Microscopy, 2022, **71(S1)**, i15–i22
DOI: https://doi.org/10.1093/jmicro/dfab053
Supplement Paper

MICROSCOPY

Cryogenic electron microscopy approaches that combine images and tilt series

Thomas Calcraft and Peter B. Rosenthal*

Structural Biology of Cells and Viruses Laboratory, The Francis Crick Institute, 1 Midland Road, London NW1 1AT, UK
*To whom correspondence should be addressed. E-mail: Peter.Rosenthal@crick.ac.uk

Abstract

Cryogenic electron microscopy can be widely applied to biological specimens from the molecular to the cellular scale. In single-particle analysis, 3D structures may be obtained in high resolution by averaging 2D images of single particles in random orientations. For pleomorphic specimens, structures may be obtained by recording the tilt series of a single example of the specimen and calculating tomograms. Where many copies of a single structure such as a protein or nucleic acid assembly are present within the tomogram, averaging of the sub-volumes (subtomogram averaging) has been successfully applied. The choice of data collection method for any given specimen may depend on the structural question of interest and is determined by the radiation sensitivity of the specimen. Here, we survey some recent developments on the use of hybrid methods for recording and analysing data from radiation-sensitive biological specimens. These include single-particle reconstruction from 2D images where additional views are recorded at a single tilt angle of the specimen and methods where image tilt series, initially used for tomogram reconstruction, are processed as individual single-particle images. There is a continuum of approaches now available to maximize structural information obtained from the specimen.

Key words: cryo-EM, cryo-ET, hybrid method, tilt series, subtomogram averaging, single-particle analysis

Introduction

The recording of images by cryogenic electron microscopy (cryo-EM) combined with image analysis has led to spectacular views of biological structure from the molecular to cellular scale. Because the images are approximately projections of the specimen, the problem of overlap may make image interpretation problematic. Single particle cryo-EM exploits the idea that low-exposure 2D images of multiple identical particles may be averaged to obtain structure in 3D. Random orientations of the particles provide all the necessary views to perform reconstruction. Where the conditions for single-particle averaging are not met, such as with a general pleomorphic specimen, additional images must be recorded by tilting the specimen holder to obtain the required views of the specimen followed by tomogram reconstruction. Because multiple images are obtained from the same object, tomogram resolution is limited by radiation damage. There are additional challenges due to the need to record multiple images of the same specimen area and to treat defocus gradients arising from the tilted specimen geometry during subsequent image processing. However, advances in microscopes and image processing software have created new opportunities for a wide range of specimen types. Furthermore, averaging repeating units within a tomogram, called subtomogram averaging, can extend the resolution for these units provided they can be aligned.

Here, we survey cryo-EM methods that obtain advantages by combining single-particle and tomographic approaches, including (i) single particle reconstruction with a specimen tilt, (ii) tomography and subtomogram averaging, (iii) single-particle tomography that directly uses 2D images, (iv) hybrid single particle tomography and (v) 2D template matching of particles in single-tilt images. Data collection geometries for these approaches are shown in Fig. 1.

Single-particle reconstruction with added tilts

Instrumental advances important to single-particle analysis include microscopes with more stable stages, better vacuums, coherent electron sources, parallel illumination, direct detectors and energy filters (see for example [1]). The most significant recent impact has come from Direct Detector Devices with improved efficiency [2] as well as the movie mode collection and frame alignment that can compensate for specimen motion [3,4]. In addition, automation has been key in the acquisition of large single-particle datasets [5].

Single-particle analysis requires the assignment of particle parameters for orientation (e.g. Euler angles (ψ, θ, φ)) and position (x, y) in the image. A wide range of orientations are required for subsequent averaging and reconstruction. High-resolution reconstructions, including those using the latest hardware and software advances to reach resolutions that resolve atomic positions [6,7], typically record images at a single orientation of the specimen stage and at several values of defocus. Correction of the contrast transfer function (CTF) is required and at higher resolution additional aberrations may also be fitted and corrected [8,9]. Classification of heterogeneity improves resolution for one or more structural

Received 11 October 2021; Revised 29 November 2021; Editorial Decision 30 November 2021; Accepted 28 January 2022

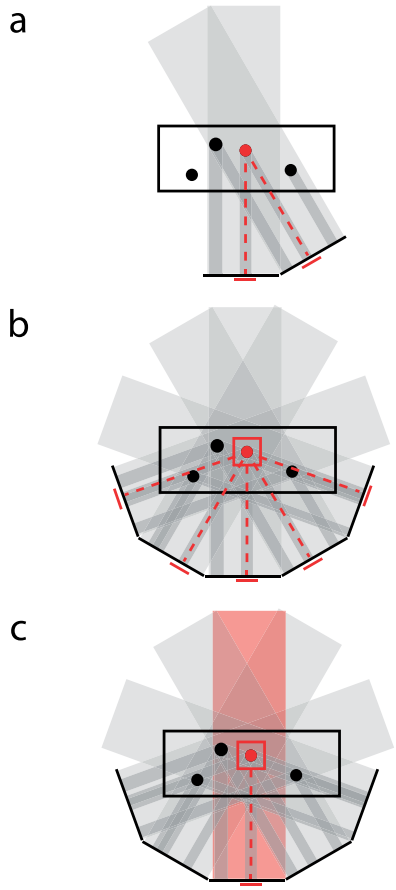

Fig. 1. Data collection schemes for cryogenic electron microscopy.

Schematic of the relationship between the tomogram/tilt series (black box/image planes) containing several particles (black circles) and the subtomogram/subtilt series (red box/red image planes) containing one particle (red circle). The 3D coordinates of a given subtomogram (red) are projected along the tilt projection vector (dashed red lines) to extract subtilt images (red image planes). Grey shaded rectangles indicate the projections from the tilt series to the tomogram. a) Tilt pairs, in which two images of the same specimen area are recorded at different orientations of the specimen holder. No tomograms or subtomograms are calculated. Particle orientations in the untilted and tilted images are related by the known tilt transformation (tilt axis and tilt angle of the specimen holder). b) Tomography with equal dose fractionation across the tilt series, with subtomograms selected for averaging and images selected for subtilt refinement. c) A high-dose, untilted image (projection direction given by the red-shaded rectangle) recorded before a low dose tilt series, with subtomogram selection for averaging and the corresponding image selected in the high-dose initial image for single particle refinement.

conformers [10,11]. Localized reconstruction may be used to isolate a molecular signal in an environment with overlap [12]. Electron beam-induced specimen motion and other effects of irradiation may reduce contrast predicted for ideal images, and finding ways to reduce this motion is an active area of research [13,14].

Single-particle specimens are most typically prepared by applying the specimen to a support containing holes and blotting and followed by plunge-freezing into liquid ethane or a propane [15] or an ethane/propane mix [16]. A thin, vitreous ice film usually provides the best images by reducing scatter from thick ice. The important requirement of a wide range of orientations may not always be met due to particles interacting with the specimen support or the air-water interface (reviewed in Glaeser [17]). This results in anisotropy of the maps which affects subsequent model building. In this case, acquiring additional images at a single tilt of the specimen holder may provide a wider range of views and restore isotropic resolution [18]. Image processing must therefore address the defocus gradient, yielding a per-particle CTF estimation [19]. Diagnosing a problem of preferred orientation from a partial dataset is important during data collection, such as with the program cryo-EF [20] so that an efficient data collection strategy including a specific tilt angle may be chosen. The assessment of anisotropy in the final map may include the calculation of a 3D Fourier Shell Correlation that describes resolution in different directions of the map [18]. Recording tomograms of a single-particle specimen may identify the distribution of particles within the sample that may explain preferred orientations, such as association with the air-water interface [21]. Experimental approaches that apply small amounts of specimen without blotting may offer advantages in addressing this problem (reviewed in [17]).

Tilt-pair analysis

In addition, images at two relative tilt angles of the specimen holder may be recorded of a single-particle field (a 'tilt-pair') as shown in the schematic in Fig. 1a. This can be used to calculate a starting model for refinement as in the first such practical scheme, the random conical tilt method [22], and the orthogonal tilt method [23]. When assigning orientations and positions to individual particles in low signal-to-noise ratio cryo-EM images, achieved by comparing projections of a 3D map to images, the alignment of noise in the image to the map projection can lead to incorrect orientations, map bias and over-fitting. A tilt-pair test may be used to validate the assignment of orientations [24–27]. Because the assigned particle orientations in the two images should be related by the transformation applied to the specimen holder during the experiment, the tilt-pair test can measure the accuracy of particle orientation determination and potentially can be used to improve it. Because the recording of the second image occurs after accumulated exposure, the particle images typically have reduced information at high resolution but orientation determination on the second image may still be performed and is informative in scoring the success of orientation determinations made on the first higher-resolution image. The tilt-pair test validates the map at low resolution by showing its consistency with image data. In Fig. 2, the tilt-pair parameter plot shows a clustering of particles at the known tilt axis and tilt angle of the experiment confirming that individual particle orientations were correctly assigned and the 3D map agrees with the images.

Hand determination

The absolute hand of a biological assembly is an important feature of its structure and function. At high resolution, such as those sufficient for building atomic models, maps reveal handed features that are directly interpretable from the map, and when incorrect, it is a simple matter to computationally invert the hand of the map. Although a low-resolution map may lack these structural details, when an atomic model for a component structure is available, this may help identify the absolute hand. Otherwise, hand determination may need to be determined experimentally, requiring image data recorded at more than one tilt angle of the specimen holder. Tilt-pair parameter plots may be used to determine the absolute hand.

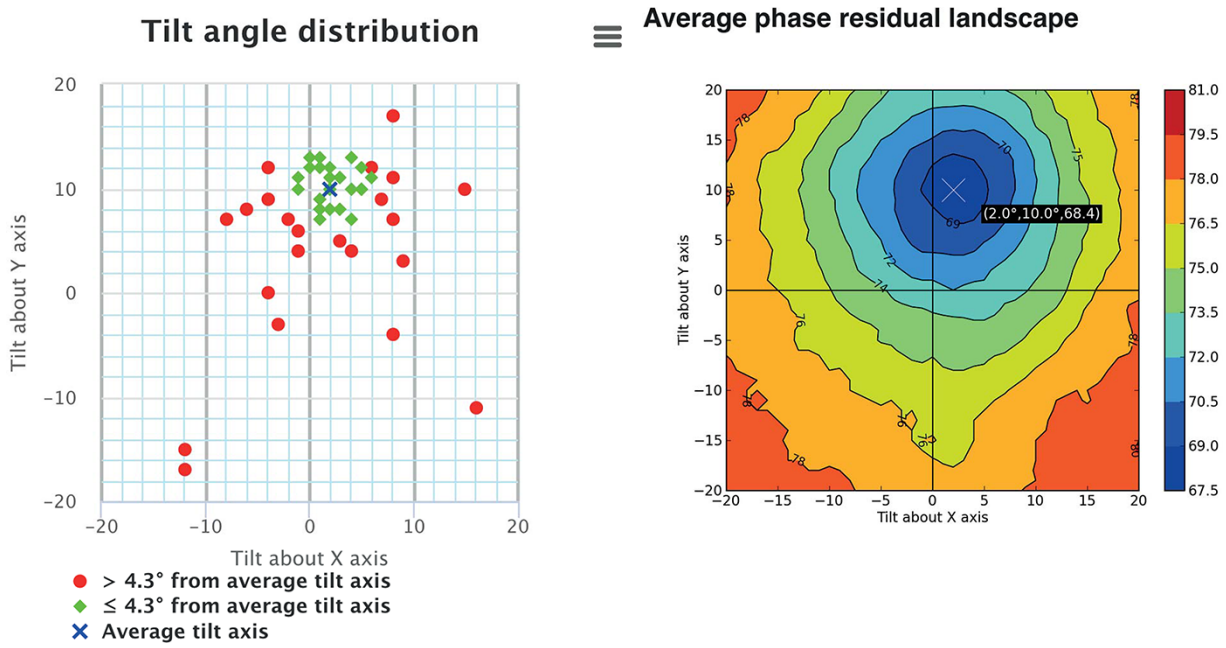

Fig. 2. Tilt-pairs analysis of a single particle structure.

Left: Each point in the plot is a transformation (rotx, roty) between particle pairs on untilted and tilted micrographs. The centre of the cluster (blue cross) is located near the known tilt axis and angle (10°) used in the experiment. **Right:** Phase residual plot indicating score (phase residual) for agreement of map projections with particle image from the tilted image after tilt transformations are applied to the orientation of the particle on the untilted image. Plot is average phase residual for 50 particles of the 1.5MDa *B. stearothermophilus* pyruvate dehydrogenase E2 core. The minimum is indicated at 10°. Plots are calculated with the tilt-validation server at the Electron Microscopy Databank at EMBL-EBI.

The calculations may be facilitated by recording a specimen of known absolute hand under identical imaging conditions or mixing together a particle of known hand with the unknown specimen.

Tilt-series for tomography and subtomogram averaging

Electron cryotomography (cryo-ET) and subtomogram averaging is currently the method of choice for the examination of macromolecular structures *in situ* [28], as the tilting of the specimen through a range of angles to record a tilt series allows complex samples to be studied in 3D (Fig. 1b and c). This avoids the problem of overlapping projections, which complicate the interpretation of 2D images without tilting. Tomography/subtomogram averaging can be the only applicable method to obtain structures of samples that cannot be purified to sufficient homogeneity for other methods such as single particle cryo-EM, X-ray crystallography, or NMR. Many thin cellular specimens as well as organelles and viruses may be prepared for tomographic imaging using methods very similar for single-particle specimens. Progress on imaging deeper in thick cellular specimens has been achieved by focussed ion beam milling of lamellae [29,30]. After the alignment of the tilt series with respect to a common frame of reference, a 3D tomogram is reconstructed, representing the specimen. Individual tomograms have a low signal-to-noise ratio and a 'missing wedge', caused by the incomplete range of tilt angles accessible in the microscope. Carrying out subtomogram averaging on identical structures found in a tomographic dataset can produce higher-resolution maps, which in principle can reach the same near-atomic resolution as single-particle analysis of purified macromolecules [31,32]. This is done by aligning 3D subtomograms to a 3D reference map and is conceptually similar to single-particle analysis, in which 2D particle images are aligned to a 3D reference map.

The advances in instrumentation that have impacted single-particle analysis have similarly impacted tomography by increasing the amount of information in images for a given electron exposure, allowing more information to be extracted from low-exposure images within a tilt series. Automation has been important for collecting optimal images throughout the tilt series [33,34]. Energy filters have impacted all types of experiments but are particularly important for the thick specimens and tilted specimens that are thick in projection.

Additional factors limit the resolution that is routinely achievable by subtomogram averaging, including but not limited to: the fractionation of the total electron dose over a tilt series and the higher doses typically used because of this, incomplete correction for beam-induced sample movement and deformation [35], errors in tilt series alignment, the rarity/heterogeneity/flexibility of the target structure, and the increased computational costs of processing 3D data as opposed to 2D [31,36]. Specific protocols for recording tomograms such as a dose-symmetric tilt series where images are recorded first at low tilt angles where the specimen is thinnest in projection and before the specimen has sustained damage have proven advantageous [37]. New collection schemes may accelerate and improve tomogram collection [38–40].

Single-particle tomography

In recent years, a number of approaches have been described for hybrid data collection/processing methods, which combine cryo-ET/subtomogram averaging data with single-particle analysis methods [36,38,41–47]. (Figs. 1b and 3)

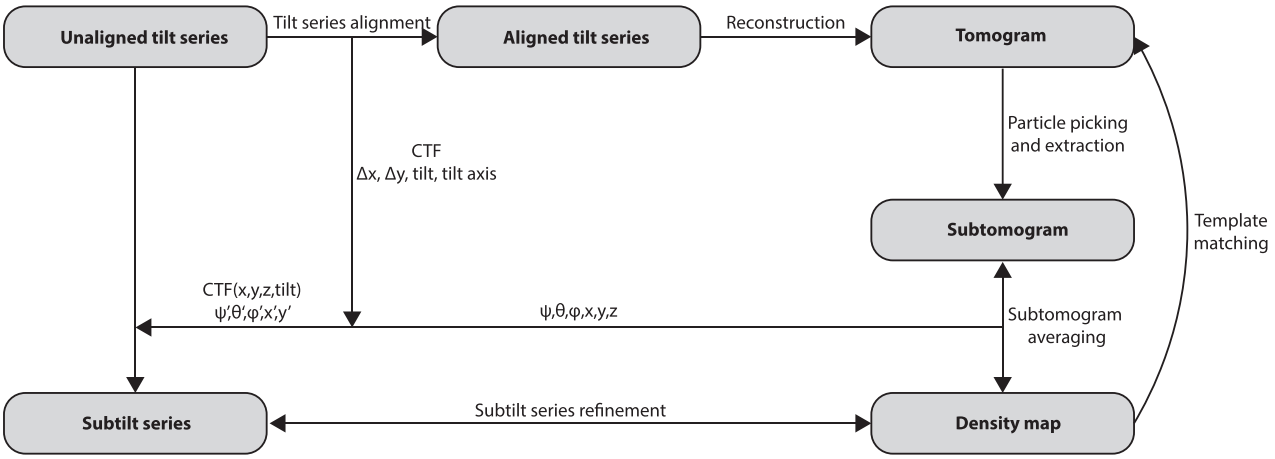

Fig. 3. Flowchart for tomography, subtomogram averaging, and subtilt reconstruction.

A map obtained by subtomogram averaging is refined against 2D projections in the subtilt series as in single particle reconstruction. The orientation and position of each subtomogram (ψ, θ, φ, x, y, z) and the tilt series alignment parameters (Δx, Δy, tilt, tilt axis) are used to assign orientation and position in the 2D images (ψ′, θ′, φ′, x, y) along with Contrast Transfer Function (CTF) parameters that are assigned as a function of x, y, z, and tilt.

While these approaches vary in their exact methods, one thing they have in common is the utilization of the 2D tilt-series image data projecting into each subtomogram (here termed a 'subtilt series' [44]), instead of using only the 3D subtomogram as in conventional subtomogram averaging. These approaches are geared towards extracting the maximum possible amount of high-resolution information present in the raw data, which might otherwise be unrecoverable. Although the first usage of subtilt series in subtomogram averaging was reported before the turn of the millennium [48], hybrid subtomogram averaging methods have only recently become available as software packages, with studies in the past 2–3 years reporting their use [43,44,47]. The further adoption of such methods promises to unify the processing of 3D subtomograms with single-particle processing of 2D particle images.

There are several advantages of using the subtilt approach as opposed to conventional subtomogram averaging:

- Constrained refinement of the orientations and shifts of each subtilt image corrects for the local beam-induced movement and distortion of the sample throughout the tilt series in addition to errors in the full-frame tilt series alignment. This process is analogous to particle polishing [49] as carried out in single-particle analysis but extending to particle rotation as well as translation while restrained by the tomographic tilt geometry.
- While tools for 3D CTF correction in cryo-ET are available [32,50], they still require development in comparison to those routinely used for 2D data in single-particle analysis and will perform sub-optimally in the case where tomograms are reconstructed with the wrong hand. Using CTF correction routines from single-particle analysis packages on the 2D subtilt data allows for full CTF correction and amplitude weighting/Wiener filtering in addition to further CTF parameter refinement [8,43,44,47].
- 3D subtomograms, like their parent tomograms, have a missing wedge of information in Fourier space, which must be accounted for during subtomogram averaging. By using the 2D subtilt images, some aspects of this problem are avoided as each image can be treated as a separate slice of Fourier space.
- Tomogram reconstruction is typically performed in real space due to the large sizes of the volumes involved. However, this introduces reconstruction artefacts [51], which are consequently also present in subtomograms. This can be avoided by making use of Fourier space reconstruction methods on the smaller subtilt images. Furthermore, the real space cropping of subtomograms from tomograms also introduces artefacts, which can be avoided by Fourier space reconstruction of subtomograms from their corresponding subtilt series. This also removes the need to reconstruct full-size unbinned tomograms, saving data storage space.
- By (i) reducing the dimensionality of the particle images from 3D to 2D (with the associated decrease in file sizes) and consequently (ii) reducing the degrees of freedom in orientational searches (ψ, θ, φ, x, y, z for 3D data, ψ, θ, φ, x, y for 2D data), the subtilt approach is less computationally intensive than 3D subtomogram averaging.
- Intermediate image interpolations (which cause some loss of high-resolution information) between the raw data and the averaged map are minimized; for conventional subtomogram averaging, interpolations are applied when transforming the raw to the aligned tilt series, reconstructing the tomogram in 3D and when reconstructing the averaged map from subtomograms. By comparison, the subtilt approach requires only one interpolation, when reconstructing the averaged map.

Ribosome data example

A demonstration of the flexibility of this single-particle tomography approach is shown by the following practical example describing how the subtomogram processing approach interfaces with single-particle processing. As an example, subtilt refinement was carried out on a test tilt-series dataset of purified ribosomes, downloaded from EMPIAR [52] (EMPIAR-10 064) (Fig. 4). This dataset, described in a study [53] that assessed the use of both the Volta-phase plate and defocused contrast in subtomogram averaging was chosen as it has been used to benchmark the hybrid processing approaches in emClarity [43], Warp/M [47] and EMAN2.3 [44].

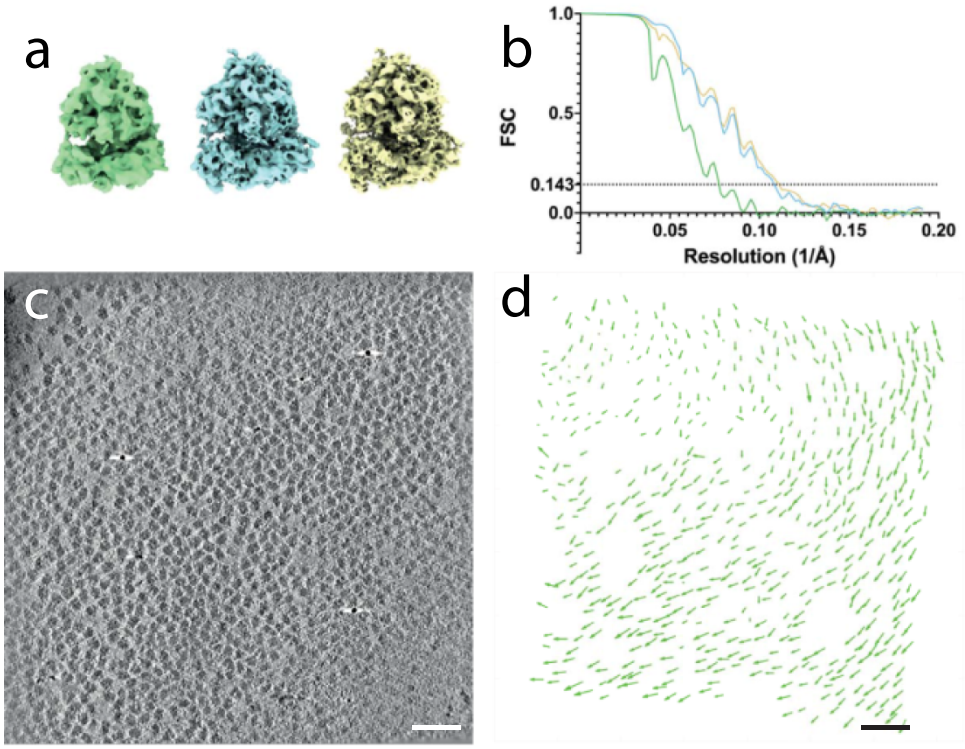

Fig. 4. Comparison of subtomogram averaging and subtilt refinement for ribosome dataset.

(a) Ribosome maps resolved from the EMPIAR-10 064 dataset. Left: 'Conventional' subtomogram averaging, resolution 13.1 Å. Middle: After subtilt refinement using images from all tilt angles in the tilt series, resolution 9.4 Å. Right: After subtilt refinement using images from tilt angles with under 30 e-/Å^2 accumulated dose, resolution 9.0 Å. (b) Relion corrected half-map FSC curves, coloured corresponding to the maps in (a). Subtilt refinement substantially improves resolution. (c) Central 10.5 Å-thick XY slice of a 4-fold binned tomogram, showing a field of ribosome particles. Scale bar is 100 nm. (d) Vector field of the residual XY shifts determined by subtilt refinement for particles in the nominal 0° tilt image from the tomogram shown in (c) (refined tilt angle of −0.41°, accumulated dose ≈16.5 e$^-$/Å^2). The mean residual shift distance is 6.9 Å; vector magnitudes have been multiplied by 10 for visualization purposes.

The EMPIAR-10 064 'mixed CTEM' dataset using defocus-based contrast [53] consisted of four tilt series of purified ribosomes with fiducial beads. The tilt series were aligned and tomograms reconstructed by weighted back projection without CTF correction using IMOD 4.9 [54]. CTF estimation was carried out using CTFFIND4 [55]. One thousand particles were then picked manually using the e2spt_boxer.py tool in EMAN2.3 [44] and subtomograms extracted in Relion 3.0 [8] to generate a reference-free initial model. This initial model was then used for template matching in EMAN2.3 (e2spt_tempmatch.py), identifying around 3300 particles. These subtomograms were then extracted in Relion 3.0, classified to remove false positives from the template matching procedure and refined against the initial model, producing a map from 3066 particles at ∼13.1 Å resolution as determined by the half-map FSC at the 0.143 threshold, similar to other conventional subtomogram averaging results from the same data [43,44] (Fig. 4). This map was compared to a published structure of the mammalian ribosome (PDB ID: 4UJE) and found to be of the wrong hand, so was subsequently mirrored in the YZ plane for further use as the reference for subtilt refinement.

Existing tilt-series alignment and CTF metadata was used to convert refined subtomogram positions and orientations to coordinates in the unaligned tilt series, as well as per-particle per-tilt Euler angles and defocus values. Dose-dependent B factors and tilt-dependent weightings were assigned to each subtilt image, following the scheme described by Bharat and Scheres [56], namely: assigning the dose-dependent B factor as 4 × (accumulated dose in e$^-$/Å^2), and the tilt-dependent weighting as cos(tilt). Subtilt images were extracted from the raw tilt-series micrographs, with Euler angles and defocus values assigned with flipped hand. The subtilt images were then refined against the subtomogram averaging map using Relion 3.0 auto-refinement, imposing a local angular search constraint of ±1° (corresponding to the 2° tomographic tilt increment) and with a translational search range of 4 pixels. Constraints on the orientation and position of the subtilt images are necessary due to the very low dose in each image, precluding full independent global alignment as carried out in single-particle analysis. This resulted in maps at 9.4 Å (using all subtilt images) and 9.0 Å (using only part of the subtilt series with ≤30 e$^-$/Å^2 accumulated dose) as determined using standard Relion postprocessing (Fig. 4). Plotting the residual shifts determined by subtilt refinement onto the 0° tilt image, corresponding to an accumulated dose of ∼16.5 e$^-$/Å^2, illustrates both the errors in tilt series alignment and the beam-induced distortion/movement of the specimen (Fig. 4d) that are corrected by subtilt refinement.

Using the same dataset, a reconstruction at a reported resolution of 5.7 Å was achieved using Warp/M [47]. An important feature of this approach is the regularization of beam-induced motion in M, in which locally correlated movements of groups of particles are used to smooth the calculated

motion trajectories. By contrast, refining each subtilt image as an independent particle does not permit the inclusion of such restraints, and greater potential for error and overfitting is introduced.

Hybrid single-particle tomography

Subtilt processing can be carried out as part of a standard tomography data processing pipeline, in which the electron dose is fractionated approximately equally across the tilt series. However, hybrid data collection strategies have recently been described, in which an initial untilted image is recorded with far higher dose, such as is typical for single-particle micrographs (Fig. 1c). By collecting a tilt series of the same field of view following this initial high-dose exposure, the orientations and positions of particles can be determined by subtomogram averaging, before extracting them from the high-dose subtilt image for the final map reconstruction [41,45,46]. This scheme has the advantage of concentrating the permissible electron dose into the highest quality image, i.e. the untilted image. This image has more signal for the estimation of microscope parameters, may be recorded closer to focus and does not suffer from the accumulated dose of the entire tilt series. Alternative data collection strategies such as these may also provide further benefits to *in situ* structure determination in the future. An experiment that records 2D images of a single-particle specimen followed by tomography of the same specimen provides a basis for comparison of the two techniques and provides an understanding of experimental issues that impact tomography and subtomogram averaging, such as the characterization of particle movements during data acquisition [57].

Template matching in 2D

While tomography overcomes the problem of overlap in projection images, another approach to study single particles in a cellular context is by detecting them in a single high-resolution 2D image of a thin cellular specimen without tilting using template matching. The goal is to identify the distribution of a known structure in a cellular context, including the presence of different conformers. This is performed by matching projections of the known structure against the 2D image. Multiple search objects can be used to identify both their orientation and conformation in the cell. This has recently included the detection of 50S ribosomal subunits by position (x, y), and orientation (ψ, θ, φ) in 2D images of *Mycoplasma pneumoniae* cells [58]. Both application and theoretical studies [59] suggest that high-resolution information and therefore close-to-focus conditions should be employed during data collection. This allows detection even in the presence of overlapping projections of objects within the sample and differs from high defocus or low-pass-filtered conditions using 3D template matching. Additionally, defocus assignment as part of this protocol provides information in 3D.

In a hybrid experiment such as that described in Fig. 1c, 2D template matching in a 2D high-resolution image may be compared to 3D template matching in a tomogram of the same specimen. In principle, this is an approach where joint 2D and 3D template matching, which may have different noise characteristics, may be used for validation and identifying false signal detection [58].

Conclusion

The advances in cryo-EM leading to increased signal in images has expanded possibilities for a wide range of experiments. Combining knowledge from images and tilt series has been informative for both single-particle analysis and tomography and has led to unified approaches in experiment and image processing. New data collection protocols may both improve image and tilt-series quality and increase throughput and will impact many structural problems, including the most difficult cases of studying molecules *in situ* in cells.

Funding

This work was supported by the Francis Crick Institute, which receives its core funding from Cancer Research UK (grant number FC001143), the UK Medical Research Council (FC001143), and the Wellcome Trust (FC001143).

Acknowledgements

We thank our colleagues for discussions. For the purpose of Open Access, the author has applied a CC BY public copyright license to any Author Accepted Manuscript version arising from this submission.

Conflict of interest

The authors declare that they have no conflict of interest.

References

1. Maki-Yonekura S, Hamaguchi T, Naitow H, Takaba K, and Yonekura K (2021) Advances in cryo-EM and ED with a cold-field emission beam and energy filtration -refinements of the CRYO ARM 300 system in RIKEN SPring-8 center. *Microscopy* 70: 232–240.
2. McMullan G, Faruqi A R, Henderson R, Guerrini N, Turchetta R, Jacobs A, and van Hoften G (2009) Experimental observation of the improvement in MTF from backthinning a CMOS direct electron detector. *Ultramicroscopy* 109: 1144–1147.
3. Campbell M G, Cheng A, Brilot A F, Moeller A, Lyumkis D, Veesler D, Pan J, Harrison S C, Potter C S, Carragher B, and Grigorieff N (2012) Movies of ice-embedded particles enhance resolution in electron cryo-microscopy. *Structure* 20: 1823–1828.
4. Li X, Mooney P, Zheng S, Booth C R, Braunfeld M B, Gubbens S, Agard D A, and Cheng Y (2013) Electron counting and beam-induced motion correction enable near-atomic-resolution single-particle cryo-EM. *Nat. Methods* 10: 584–590.
5. Tan Y Z, Cheng A, Potter C S, and Carragher B (2016) Automated data collection in single particle electron microscopy. *Microscopy* 65: 43–56.
6. Nakane T, Kotecha A, Sente A, McMullan G, Masiulis S, Brown P, Grigoras I T, Malinauskaite L, Malinauskas T, Miehling J, Uchanski T, Yu L, Karia D, Pechnikova E V, de Jong E, Keizer J, Bischoff M, McCormack J, Tiemeijer P, Hardwick S W, Chirgadze D Y, Murshudov G, Aricescu A R, and Scheres S H W (2020) Single-particle cryo-EM at atomic resolution. *Nature* 587: 152–156.
7. Yip K M, Fischer N, Paknia E, Chari A, and Stark H (2020) Atomic-resolution protein structure determination by cryo-EM. *Nature* 587: 157–161.
8. Zivanov J, Nakane T, Forsberg B O, Kimanius D, Hagen W J, Lindahl E, and Scheres S H (2018) New tools for automated high-resolution cryo-EM structure determination in RELION-3. *Elife* 7: e42166.

9. Zivanov J, Nakane T, and Scheres S H W (2020) Estimation of high-order aberrations and anisotropic magnification from cryo-EM data sets in RELION-3.1. *IUCrJ* 7: 253–267.
10. Lyumkis D, Brilot A F, Theobald D L, and Grigorieff N (2013) Likelihood-based classification of cryo-EM images using FREALIGN. *J. Struct. Biol.* 183: 377–388.
11. Scheres S H, Gao H, Valle M, Herman G T, Eggermont P P, Frank J, and Carazo J M (2007) Disentangling conformational states of macromolecules in 3D-EM through likelihood optimization. *Nat. Methods* 4: 27–29.
12. Ilca S L, Kotecha A, Sun X, Poranen M M, Stuart D I, and Huiskonen J T (2015) Localized reconstruction of subunits from electron cryomicroscopy images of macromolecular complexes. *Nat. Commun.* 6: 8843.
13. Naydenova K, Jia P, and Russo C J (2020) Cryo-EM with sub-1 A specimen movement. *Science* 370: 223–226.
14. Russo C J and Passmore L A (2016) Progress towards an optimal specimen support for electron cryomicroscopy. *Curr. Opin. Struct. Biol.* 37: 81–89.
15. Dubochet J, Adrian M, Chang J J, Homo J C, Lepault J, McDowall A W, and Schultz P (1988) Cryo-electron microscopy of vitrified specimens. *Q. Rev. Biophys.* 21: 129–228.
16. Tivol W F, Briegel A, and Jensen G J (2008) An improved cryogen for plunge freezing. *Microsc. Microanal.* 14: 375–379.
17. Glaeser R M (2021) Preparing better samples for cryo-electron microscopy: biochemical challenges do not end with isolation and purification. *Annu. Rev. Biochem.* 90: 451–474.
18. Tan Y Z, Baldwin P R, Davis J H, Williamson J R, Potter C S, Carragher B, and Lyumkis D (2017) Addressing preferred specimen orientation in single-particle cryo-EM through tilting. *Nat. Methods* 14: 793–796.
19. Su M (2019) goCTF: geometrically optimized CTF determination for single-particle cryo-EM. *J. Struct. Biol.* 205: 22–29.
20. Naydenova K and Russo C J (2017) Measuring the effects of particle orientation to improve the efficiency of electron cryomicroscopy. *Nat. Commun.* 8: 629.
21. Noble A J, Dandey V P, Wei H, Brasch J, Chase J, Acharya P, Tan Y Z, Zhang Z, Kim L Y, Scapin G, Rapp M, Eng E T, Rice W J, Cheng A, Negro C J, Shapiro L, Kwong P D, Jeruzalmi D, des Georges A, Potter C S, and Carragher B (2018) Routine single particle CryoEM sample and grid characterization by tomography. *Elife* 7: e34257.
22. Radermacher M, Wagenknecht T, Verschoor A, and Frank J (1986) A new 3-D reconstruction scheme applied to the 50S ribosomal subunit of E. coli. *J. Microsc.* 141: RP1–2.
23. Leschziner A E and Nogales E (2006) The orthogonal tilt reconstruction method: an approach to generating single-class volumes with no missing cone for ab initio reconstruction of asymmetric particles. *J. Struct. Biol.* 153: 284–299.
24. Henderson R, Chen S, Chen J Z, Grigorieff N, Passmore L A, Ciccarelli L, Rubinstein J L, Crowther R A, Stewart P L, and Rosenthal P B (2011) Tilt-pair analysis of images from a range of different specimens in single-particle electron cryomicroscopy. *J. Mol. Biol.* 413: 1028–1046.
25. Rosenthal P B and Henderson R (2003) Optimal determination of particle orientation, absolute hand, and contrast loss in single-particle electron cryomicroscopy. *J. Mol. Biol.* 333: 721–745.
26. Russo C J and Passmore L A (2014) Robust evaluation of 3D electron cryomicroscopy data using tilt-pairs. *J. Struct. Biol.* 187: 112–118.
27. Wasilewski S and Rosenthal P B (2014) Web server for tilt-pair validation of single particle maps from electron cryomicroscopy. *J. Struct. Biol.* 186: 122–131.
28. Bauerlein F J B and Baumeister W (2021) Towards visual proteomics at high resolution. *J. Mol. Biol.* 433: 167187.
29. Schaffer M, Mahamid J, Engel B D, Laugks T, Baumeister W, and Plitzko J M (2017) Optimized cryo-focused ion beam sample preparation aimed at in situ structural studies of membrane proteins. *J. Struct. Biol.* 197: 73–82.
30. Mahamid J, Pfeffer S, Schaffer M, Villa E, Danev R, Cuellar L K, Forster F, Hyman A A, Plitzko J M, and Baumeister W (2016) Visualizing the molecular sociology at the HeLa cell nuclear periphery. *Science* 351: 969–972.
31. Briggs J A (2013) Structural biology in situ—the potential of subtomogram averaging. *Curr. Opin. Struct. Biol.* 23: 261–267.
32. Turonova B, Schur F K M, Wan W, and Briggs J A G (2017) Efficient 3D-CTF correction for cryo-electron tomography using NovaCTF improves subtomogram averaging resolution to 3.4A. *J. Struct. Biol.* 199: 187–195.
33. Mastronarde D N (2005) Automated electron microscope tomography using robust prediction of specimen movements. *J. Struct. Biol.* 152: 36–51.
34. Suloway C, Shi J, Cheng A, Pulokas J, Carragher B, Potter C S, Zheng S Q, Agard D A, and Jensen G J (2009) Fully automated, sequential tilt-series acquisition with Leginon. *J. Struct. Biol.* 167: 11–18.
35. Fernandez J J, Li S, Bharat T A M, and Agard D A (2018) Cryotomography tilt-series alignment with consideration of the beam-induced sample motion. *J. Struct. Biol.* 202: 200–209.
36. Bartesaghi A, Lecumberry F, Sapiro G, and Subramaniam S (2012) Protein secondary structure determination by constrained single-particle cryo-electron tomography. *Structure* 20: 2003–2013.
37. Hagen W J H, Wan W, and Briggs J A G (2017) Implementation of a cryo-electron tomography tilt-scheme optimized for high resolution subtomogram averaging. *J. Struct. Biol.* 197: 191–198.
38. Bouvette J, Liu H F, Du X, Zhou Y, Sikkema A P, da Fonseca Rezende E M J, Klemm B P, Huang R, Schaaper R M, Borgnia M J, and Bartesaghi A (2021) Beam image-shift accelerated data acquisition for near-atomic resolution single-particle cryo-electron tomography. *Nat. Commun.* 12: 1957.
39. Chreifi G, Chen S, Metskas L A, Kaplan M, and Jensen G J (2019) Rapid tilt-series acquisition for electron cryotomography. *J. Struct. Biol.* 205: 163–169.
40. Eisenstein F, Danev R, and Pilhofer M (2019) Improved applicability and robustness of fast cryo-electron tomography data acquisition. *J. Struct. Biol.* 208: 107–114.
41. Bharat T A, Davey N E, Ulbrich P, Riches J D, de Marco A, Rumlova M, Sachse C, Ruml T, and Briggs J A (2012) Structure of the immature retroviral capsid at 8Å resolution by cryo-electron microscopy. *Nature* 487: 385–389.
42. Zhang L and Ren G (2012) IPET and FETR: experimental approach for studying molecular structure dynamics by cryo-electron tomography of a single-molecule structure. *PLoS One* 7: e30249.
43. Himes B A and Zhang P (2018) emClarity: software for high-resolution cryo-electron tomography and subtomogram averaging. *Nat. Methods* 15: 955–961.
44. Chen M, Bell J M, Shi X, Sun S Y, Wang Z, and Ludtke S J (2019) A complete data processing workflow for cryo-ET and subtomogram averaging. *Nat. Methods* 16: 1161–1168.
45. Song K, Shang Z, Fu X, Lou X, Grigorieff N, and Nicastro D (2020) In situ structure determination at nanometer resolution using TYGRESS. *Nat. Methods* 17: 201–208.
46. Sanchez R M, Zhang Y, Chen W, Dietrich L, and Kudryashev M (2020) Subnanometer-resolution structure determination in situ by hybrid subtomogram averaging - single particle cryo-EM. *Nat. Commun.* 11: 3709.

47. Tegunov D, Xue L, Dienemann C, Cramer P, and Mahamid J (2021) Multi-particle cryo-EM refinement with M visualizes ribosome-antibiotic complex at 3.5 A in cells. *Nat. Methods* 18: 186–193.
48. Walz J, Typke D, Nitsch M, Koster A J, Hegerl R, and Baumeister W (1997) Electron tomography of single ice-embedded macromolecules: Three- dimensional alignment and classification. *J. Struct. Biol.* 120: 387–395.
49. Zivanov J, Nakane T, and Scheres S H W (2019) A Bayesian approach to beam-induced motion correction in cryo-EM single-particle analysis. *IUCrJ* 6: 5–17.
50. Xiong Q, Morphew M K, Schwartz C L, Hoenger A H, and Mastronarde D N (2009) CTF determination and correction for low dose tomographic tilt series. *J. Struct. Biol.* 168: 378–387.
51. Turonova B, Marsalek L, and Slusallek P (2016) On geometric artifacts in cryo electron tomography. *Ultramicroscopy* 163: 48–61.
52. Iudin A, Korir P K, Salavert-Torres J, Kleywegt G J, and Patwardhan A (2016) EMPIAR: a public archive for raw electron microscopy image data. *Nat. Methods* 13: 387–388.
53. Khoshouei M, Pfeffer S, Baumeister W, Forster F, and Danev R (2017) Subtomogram analysis using the volta phase plate. *J. Struct. Biol.* 197: 94–101.
54. Kremer J, Mastronarde D N, and McIntosh J (1996) Computer visualization of three-dimensional image data using IMOD. *J. Struct. Biol.* 116: 71–76.
55. Rohou A and Grigorieff N (2015) CTFFIND4: fast and accurate defocus estimation from electron micrographs. *J. Struct. Biol.* 192: 216–221.
56. Bharat T A and Scheres S H (2016) Resolving macromolecular structures from electron cryo-tomography data using subtomogram averaging in RELION. *Nat. Protoc.* 11: 2054–2065.
57. Bharat T A M, Russo C J, Lowe J, Passmore L A, and Scheres S H W (2015) Advances in single-particle electron cryomicroscopy structure determination applied to sub-tomogram averaging. *Structure* 23: 1743–1753.
58. Lucas B A, Himes B A, Xue L, Grant T, Mahamid J, and Grigorieff N (2021) Locating macromolecular assemblies in cells by 2D template matching with cisTEM. *Elife* 10: e68946.
59. Rickgauer J P, Grigorieff N, and Denk W (2017) Single-protein detection in crowded molecular environments in cryo-EM images. *Elife* 6: e25648.